THE JOURNAL OF BIOLOGICAL CHEMISTRY VOL. 286, NO. 51, pp. 44015–44022, December 23, 2011
© 2011 by The American Society for Biochemistry and Molecular Biology, Inc. Printed in the U.S.A.

Nuclear Localization of *de Novo* Thymidylate Biosynthesis Pathway Is Required to Prevent Uracil Accumulation in DNA*

Received for publication, September 26, 2011, and in revised form, October 14, 2011 Published, JBC Papers in Press, November 4, 2011, DOI 10.1074/jbc.M111.307629

Amanda J. MacFarlane[‡1], Donald D. Anderson[§], Per Flodby[‡2], Cheryll A. Perry[‡], Robert H. Allen[¶], Sally P. Stabler[¶], and Patrick J. Stover[‡§3]

From the [‡]Division of Nutritional Sciences, Cornell University, Ithaca, New York 14853, the [§]Graduate Field of Biochemistry, Molecular and Cell Biology, Cornell University, Ithaca, New York 14853, and the [¶]Department of Medicine and Division of Hematology, University of Colorado School of Medicine, Aurora, Colorado 80045

Background: S phase nuclei contain the thymidylate synthesis pathway.
Results: Mice overexpressing a *Shmt1* transgene exhibit elevated expression of SHMT1 and TYMS, impaired nuclear localization of the thymidylate biosynthesis pathway, and elevated uracil in DNA.
Conclusion: SHMT1 and TYMS localization to the nucleus is essential to prevent uracil accumulation in DNA.
Significance: SHMT1-mediated nuclear *de novo* thymidylate synthesis is critical for maintaining DNA integrity.

Uracil accumulates in DNA as a result of impaired folate-dependent *de novo* thymidylate biosynthesis, a pathway composed of the enzymes serine hydroxymethyltransferase (SHMT), thymidylate synthase (TYMS), and dihydrofolate reductase. In G_1, this pathway is present in the cytoplasm and at S phase undergoes small ubiquitin-like modifier-dependent translocation to the nucleus. It is not known whether this pathway functions in the cytoplasm, nucleus, or both *in vivo*. SHMT1 generates 5,10-methylenetetrahydrofolate for *de novo* thymidylate biosynthesis, a limiting step in the pathway, but also tightly binds 5-methyltetrahydrofolate in the cytoplasm, a required cofactor for homocysteine remethylation. Overexpression of SHMT1 in cell cultures inhibits folate-dependent homocysteine remethylation and enhances thymidylate biosynthesis. In this study, the impact of increased *Shmt1* expression on folate-mediated one-carbon metabolism was determined in mice that overexpress the *Shmt1* cDNA (*Shmt1*$^{tg+}$ mice). Compared with wild type mice, *Shmt1*$^{tg+}$ mice exhibited elevated SHMT1 and TYMS protein levels in tissues and evidence for impaired homocysteine remethylation but surprisingly exhibited depressed levels of nuclear SHMT1 and TYMS, lower rates of nuclear *de novo* thymidylate biosynthesis, and a nearly 10-fold increase in uracil content in hepatic nuclear DNA when fed a folate- and choline-deficient diet. These results demonstrate that SHMT1 and TYMS localization to the nucleus is essential to prevent uracil accumulation in nuclear DNA and indicate that SHMT1-mediated nuclear *de novo* thymidylate synthesis is critical for maintaining DNA integrity.

Depletion of *de novo* dTMP synthesis caused by folate deficiency, antifolate inhibitors, or genetic disruption of the pathway results in deoxyuridine misincorporation into nuclear DNA leading to genome instability (1–3). *De novo* thymidylate biosynthesis is distinct from the other nucleotide synthesis pathways in that it is compartmentalized at the sites of DNA replication, namely the mitochondria (4) and nucleus (5, 6). The *de novo* thymidylate biosynthesis pathway requires three enzymatic activities: serine hydroxymethyltransferase (SHMT),[4] which catalyzes the conversion of serine and tetrahydrofolate (THF) to form glycine and methyleneTHF; thymidylate synthase (TYMS), which catalyzes the conversion of methyleneTHF and dUMP to dTMP; and dihydrofolate (DHF). The cycle is completed by the conversion of DHF to THF in a NADPH-requiring reaction catalyzed by dihydrofolate reductase (DHFR) (Fig. 1). In mitochondria, the pathway is encoded by *SHMT2*, *TYMS*, and *DHFR1* (4). Disruption of the pathway in Chinese hamster ovary cell mitochondria results in a glycine auxotrophy and elevated levels of uracil in mitochondrial DNA (4). In the nucleus, the *de novo* thymidylate biosynthesis pathway is encoded by *SHMT1* and, to a lesser extent *SHMT2*, which are functionally redundant in supplying methyleneTHF, *TYMS*, and *DHFR*. *TYMS* is the only gene that is common to and essential for mitochondrial and nuclear thymidylate biosynthesis and is essential for early embryonic development (7).

Nuclear thymidylate biosynthesis is cell cycle-regulated through the small ubiquitin-like modifier (SUMO)-dependent nuclear translocation of SHMT1, TYMS, and DHFR during S phase (5, 6, 8). Isolated intact nuclei exhibit *de novo* thymidylate synthesis activity, but this activity is lost in sonicated nuclei, suggesting that this pathway functions through a multienzyme complex and requires compartmentalization in an intact nucleus (8). It is not known whether thymidylate biosynthesis occurs in the cytoplasm. *Shmt1*$^{-/-}$ mice are viable and fertile

* This work was supported by Public Health Service Grant DK58144.
[1] Present address: Nutrition Research Division, Food Directorate, Health Products and Food Branch, Health Canada, Ottawa, Ontario K1A 0K9, Canada
[2] Present address: Division of Pulmonary & Critical Care Medicine, Keck School of Medicine, University of Southern California, 2011 Zonal Ave., HMR 911, Los Angeles, CA 90033.
[3] To whom correspondence should be addressed: 315 Savage Hall, Division of Nutritional Sciences, Cornell University, Ithaca NY 14853. Tel.: 607-255-9751; Fax 607-255-1033; E-mail: pjs13@cornell.edu.

[4] The abbreviations used are: SHMT, serine hydroxymethyltransferase; AdoHcy, *S*-adenosylhomocysteine; AdoMet, *S*-adenosylmethionine; DHF, dihydrofolate; DHFR, DHF reductase; SUMO, small ubiquitin-like modifier; THF, tetrahydrofolate; TYMS, thymidylate synthase; ANOVA, analysis of variance.

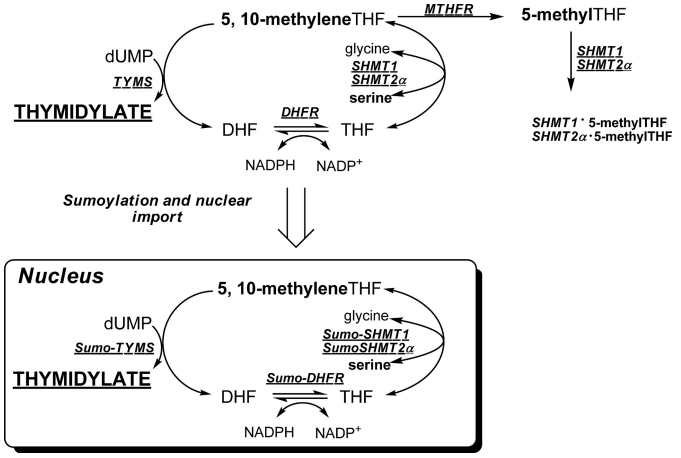

FIGURE 1. **Folate-dependent *de novo* thymidylate biosynthesis.** The *de novo* thymidylate biosynthesis pathway is comprised of SHMT1, SHMT2α, TYMS, and DHFR. During the S phase, these enzymes are sumoylated by Ubc9, which serves as a signal for nuclear import.

(3) and retain about 25% *de novo* thymidylate biosynthesis capacity in isolated hepatic nuclei because of redundant function of the enzyme SHMT2α, encoded by *Shmt2* through alternative promoter usage (8). Despite this functional redundancy between SHMT1 and SHMT2α in the cytoplasm and nucleus, SHMT1 is the major provider of methyleneTHF; mice are sensitive to reductions in SHMT1 expression, as indicated by elevated levels of uracil in nuclear DNA in $Shmt1^{+/-}$ mice (3, 9), and their increased susceptibility to neural tube defects (10) and $Apc^{min/+}$-mediated intestinal tumors (9). Interestingly, a common *SHMT1* human variant, L474F, is not an effective substrate for UBC-9-catalyzed sumoylation *in vitro* and exhibits impaired nuclear translocation at S phase (8), suggesting that its association with cardiovascular disease (11, 12) and lung cancer (13) risk may be due to impaired nuclear *de novo* thymidylate synthesis.

SHMT1 activity can be limiting for nuclear *de novo* thymidylate biosynthesis and is also involved in homocysteine remethylation in the cytoplasm. Expression of the SHMT1 cDNA in cell cultures increases rates of *de novo* thymidylate biosynthesis, while impairing homocysteine remethylation (14). SHMT1 impairs folate-dependent homocysteine remethylation in the cytoplasm by binding and sequestering 5-methylTHF, the substrate for methionine synthase, thereby making it unavailable for the homocysteine remethylation cycle (Fig. 1) (3, 14). SHMT1 expression is regulated over a wide dynamic range in cell culture models by zinc chelators (15), ferritin (16), UV radiation (17), and vitamin A (18), but the effects of increased SHMT1 expression on one-carbon metabolism have not been examined in an animal model. Here, we have generated a transgenic mouse model that overexpresses SHMT1, $Shmt1^{tg+}$ mice, to determine the impact of elevated SHMT1 expression on homocysteine remethylation and *de novo* thymidylate synthesis *in vivo*. In this mouse model, increased SHMT1 expression impaired nuclear localization of the *de novo* dTMP synthesis pathway and markedly increased uracil accumulation in nuclear DNA, indicating an essential role for nuclear thymidylate biosynthesis in the maintenance of DNA integrity and suggests that *de novo* thymidylate biosynthesis does not occur in the cytoplasm at rates sufficient to prevent uracil misincorporation into DNA.

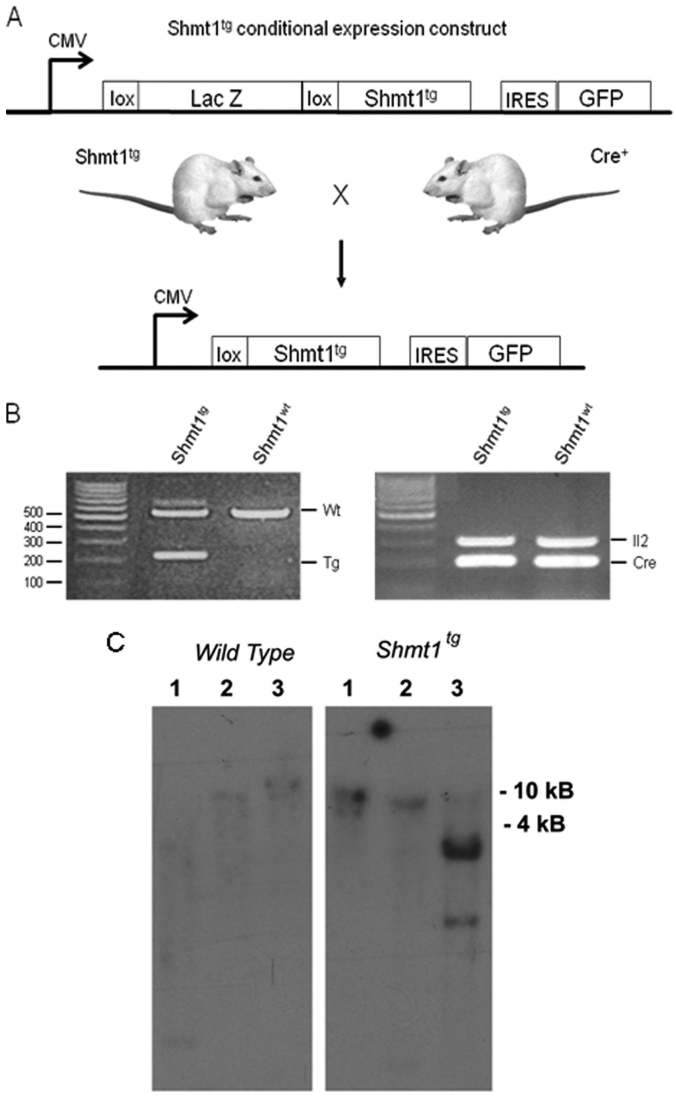

FIGURE 2. **Generation of SHMT1 overexpressing mice.** *A*, an inducible βgeo/*Shmt1* expression vector was created to allow for Cre/lox activation of the *Shmt1* transgene. The βgeo/*Shmt1* expression cassette allows for detection and localization of the transgene promoter activity via the *lacZ* reporter gene and for conditional overexpression of functional SHMT1. Transgene activation is achieved when $Shmt1^{tg}$ mice are mated to Cre-expressing mice, in this case, *Cre* expression was controlled by the CMV promoter. *Cre* expression results in the deletion of the *βgeo* reporter gene while simultaneously repositioning the *Shmt1* transgene 3′ of the chicken β-actin promoter; we refer to mice expressing *Cre* and the transgene as $Shmt1^{tg+}$. *B*, $Shmt1^{tg+}$ genotyping in Cre^{+} *Shmt1* wild type mice and Cre^{+} $Shmt1^{tg+}$ SHMT1 overexpressing mice. The *Shmt1* transgene is detected as a 215-bp PCR product, whereas the wild type (*Wt*) allele is detected as a 542-bp PCR product. The presence of the *Cre* transgene was detected as a 119-bp PCR product, and the *Il2* internal control gene was detected as a 324-bp PCR product. *C*, Southern blot of genomic DNA demonstrating a single insertion of the *Shmt1* transgene. Total nuclear DNA from tail snips was isolated from PCR verified $Shmt1^{wt}$ and $Shmt1^{tg}$ mice. The DNA was digested with BglII (*lane 1*, does not cut within the Z/EG vector), EcoR5 (*lane 2*, does not cut the Z/EG vector but cuts at position 418nt of the *Shmt1* cDNA), or XhoI (*lane 3*, the site used for cloning that cuts 5′ and 3′ of the *Shmt1* cDNA insert within the vector). $Shmt1^{wt+}$, Cre^{+} *Shmt1* wild type mice; $Shmt1^{tg+}$, Cre^{+} $Shmt1^{tg}$ mice.

EXPERIMENTAL PROCEDURES

Shmt1 Expression Vector—The *Shmt1* Z/EG vector (Fig. 2*A*) was designed to express the βgeo reporter cassette under the

control of the chicken β-actin promoter. The Z/EG vector contains the chicken β-actin promoter with an upstream cytomegalovirus enhancer that drives the expression of a *lox*P-flanked βgeo cassette (*lacZ*-neomycin resistance fusion) and an internal ribosome entry sequence that enables the translation of an enhanced GFP (19). The murine *Shmt1* cDNA (20) was cloned 3′ of the second *lox*P site and 5′ of the internal ribosome entry sequence-enhanced GFP into the XhoI site (Fig. 2*A*). Following Cre-mediated excision, the murine *Shmt1* cDNA is located directly 3′ of the β-actin promoter.

Generation of Shmt1^{tg} Mice—Mice were maintained under specific pathogen-free conditions in accordance with standard use protocols and animal welfare regulations. All of the study protocols were approved by the Institutional Animal Care and Use Committee of Cornell University and conform to the National Institutes of Health Guide for the Care and Use of Laboratory Animals. The Z/EG vector containing the *Shmt1* cDNA was linearized with SfiI, which cuts 3′ of the enhanced GFP cDNA. *Shmt1^{tg}* mice were generated by pronuclear injection of the linearized construct into FVB/N embryos at the Cornell University Transgenic Mouse Facility. Single site integration of the vector was confirmed in *Shmt1^{tg}* founder mice by Southern blot analysis of purified tail DNA (Qiagen) (Fig. 2*C*). Total nuclear DNA was digested with: BglII, which does not cut within the *Shmt*1 cDNA or the vector; EcoR5, which cuts at nucleotide 418 of the *Shmt1* cDNA but not in the vector; or XhoI, which was the cloning site for the *Shmt1* cDNA insertion into the vector. The digests were run on a 1.5% agarose gel, transferred to nitrocellulose, and hybridized with a ^{32}P-labeled probe generated from nucleotides 443–1233 of the *Shmt1* cDNA using protocols described elsewhere (21). DNA isolated from the FVB/N-Tg(ACTB-LacZ/Shmt1)B1Stov (*Shmt1^{tg}*) founder exhibited a high molecular band when digested with BglII or EcoR5. Digestion with XhoI resulted in a prominent band of 1.6 kb and a weaker smaller band, which were not observed in DNA isolated from wild type mice (Fig. 2*C*). The major 1.6-kb band approximates the size of the *Shmt1* cDNA insert, whereas the smaller minor band likely reflects XhoI star activity. Southern blots were repeated over three generations without changes in the Southern banding pattern, indicating a single integration site. A single male founder was used to generate the colony. Thereafter, *Shmt1^{tg}* mice were genotyped by PCR using purified tail nuclear DNA (Qiagen) using the forward primer 5′-gatcccaagactggcaaagagactt-3′ and the reverse primer 5′-gatgcactcacagagctaggctacaaa-3′, which correspond to exon 9 and 10, respectively, of the *Shmt1* gene, which amplify 215- and 542-bp products representing the Shmt1 transgene and wild type alleles (Fig. 2*B*).

To achieve cDNA activation, *loxP* sites were placed both 5′ and 3′ of the *βgeo* cassette. The *Shmt1* transgene was activated by crossing male FVB/N-Tg(ACTB-LacZ/Shmt1)B1Stov (*Shmt1^{tg}*) mice with female BALB/c-Tg(CMV-Cre)1Cgn/J (Cre; The Jackson Laboratory, Bar Harbor, ME) mice that were homozygous for the *Cre* transgene. Presence of the *Cre* allele was determined by PCR using the forward primer 5′-ACCAGCCAGCTATCAACTCG-3′ and the reverse primer 5′-TTACATTGGTCCAGCCACC-3′, as described (The Jackson Laboratory). The forward and reverse primers 5′-CTAGGCCACAGAATTGAAAGATCT-3′ and 5′-GTAGGTGGAAATTCTAGCATCATCC-3′, respectively, were used for detection of the *Il2* internal control gene, as described (The Jackson Laboratory) (Fig. 2*B*).

Diets—Mice used for characterization of protein overexpression and the nuclear dTMP synthesis assays were fed a standard rodent chow (Harlan Teklad LM-485) from weaning. Mice on the controlled diet study were randomly weaned at 3 weeks of age to a control diet (AIN93G containing 2 mg of folic acid/kg and 2.5 g of choline bitartrate/kg; Dyets, Inc., Bethlehem, PA) or a folate/choline-deficient diet (AIN-93G diet lacking folic acid and choline; Dyets, Inc.). The mice were maintained on the controlled diet for 5 or 32 weeks (until 8 or 35 weeks of age), as indicated in the results.

Determination of AdoMet and AdoHcy Concentrations—The animal feeding cycle was synchronized prior to tissue harvest to ensure AdoMet concentrations reflected homocysteine remethylation capacity with minimal contributions from dietary methionine. Food was removed 24 h prior to killing the animals. After 12 h, each animal was given one food pellet, and the animals were killed 12 h later by cervical dislocation. Tissues were harvested and immediately flash-frozen and stored at −80 °C until analysis. Frozen tissues were sonicated in 500 μl of 0.1 M NaAcO buffer (pH 6), and protein was precipitated by adding 312 μl of 10% perchloric acid to each sample. After vortexing, samples were centrifuged at 2000 × *g* for 10 min at 4 °C. AdoMet and AdoHcy were determined as described previously (14). AdoMet and AdoHcy values were normalized to total protein (22).

Immunoblotting—For tissues, total protein was extracted and quantified by the Lowry-Bensadoun assay (22). Tissue lysis was achieved by sonication in lysis buffer (2% SDS, 100 mM, dithiothreitol, 60 mM Tris, pH 6.8). For analysis of liver nuclei, pelleted nuclei, purified as described below, were disrupted by boiling in SDS-PAGE loading buffer for 10 min, and protein concentrations were quantified.

Proteins (40 μg/well for tissues, 20 μg/well for nuclei) were separated on a 10% (nuclei) or 12% (tissue) SDS-PAGE gel. Proteins were transferred at 4 °C to an Immobilon-P polyvinylidene difluoride membrane (Millipore Corp.) using a Transblot apparatus (Bio-Rad). Following transfer, the membranes were blocked in 5% (w/v) nonfat skim milk in PBS for 1 h followed by overnight incubation in primary antibody at 4 °C. The membranes were washed with PBS containing 0.1% Tween 20 and then incubated overnight with the appropriate horseradish peroxidase-conjugated secondary antibody (below). The membranes were visualized using the SuperSignal® West Pico chemiluminescent substrate system (Pierce).

For SHMT1 detection, sheep anti-mouse SHMT1 antibody (20) was diluted 1:10,000, and rabbit anti-sheep IgG secondary antibody (Pierce) was diluted 1:20,000. For TYMS detection, affinity-purified sheep anti-human TS antibody (Abcam) was diluted 1:5000, and rabbit anti-sheep IgG secondary antibody (Pierce) was diluted 1:10,000. For DHFR detection, affinity-purified goat anti-human DHFR antibody (Santa Cruz Biotechnology) was diluted 1:1000, and mouse anti-goat IgG secondary antibody (Pierce) was diluted 1:5000. For lamin A detection, rabbit anti-lamin A (Santa Cruz Biotechnology) was diluted

1:500, and goat anti-rabbit IgG secondary antibody (Pierce) was diluted 1:20000. For detection of the loading control GAPDH, mouse anti-human GAPDH antibody (Novus Biologicals) was diluted 1:100,000 dilution, and goat anti-mouse IgG secondary antibody (Pierce) was diluted 1:10000.

Plasma and Tissue Folate Concentration—Folate concentration in plasma and liver was quantified using the *Lactobacillus casei* microbiological assay as described (14).

For quantification of nuclear folate levels, four livers were isolated from *Shmt1*$^{wt+}$ and *Shmt1*$^{tg+}$ mice and placed immediately in cold PBS at 5 °C containing 200 mM β-mercaptoethanol (Sigma) and 2% (w/v) sodium ascorbate (Sigma). Liver nuclei from four age-matched males for each genotype were combined and prepared as described under "Nuclear *de Novo* Thymidylate Synthesis." Nuclear folate content was determined in two independent experiments.

Uracil Content in Nuclear DNA—Nuclear DNA was extracted from 25–50 mg of tissue using DNeasy Tissue and Blood Kit (Qiagen), including an incubation with RNase A (Sigma) and RNase T1 (Ambion) for 30 min at 37 °C. 10 μg of DNA was treated with 1 unit of uracil DNA glycosylase (Epicenter) for 1 h at 37 °C. Immediately following incubation, 10 pg of [$^{15}N_2$]uracil (Cambridge Isotopes) was added to each sample as an internal standard, and the sample was dried completely in a speed vacuum. 50 μl of acetonitrile, 10 μl of triethylamine, and 1 μl of 3,5-bis(trifluoromethyl) benzyl bromide were added to each sample and incubated for 25 min at 30 °C with shaking at 500 rpm. 50 μl of water followed by 100 μl of isooctane were added to each sample. The samples were vortexed and centrifuged. Organic extraction of derived uracil was completed by the removal of the aqueous phase and analysis of the organic phase.

Analysis of uracil-3,5-bis(trifluoromethyl) benzyl bromide was carried out on a Shimadzu QP2010. 1 μl of sample or standard was analyzed in the splitless mode with a purge activation time of 1 min and split vent flow of 50 ml/min with an injection port temperature of 280 °C. Ultrapurity helium gas was used as carrier gas with a linear velocity of 55 ml/min. Separation of derived uracil was obtained by using an XTI-5, 30 m, 0.25-mm inner diameter, 0.25-μm column (Restek), using the following temperature cycles for the oven: 100 °C for 1 min, ramping to 280 °C at 25 °C/min, holding for 5 min, ramping to 300 °C at 5 °C/min, and holding for 5 min. The interface temperature was held at 300 °C with an ion source temperature of 260 °C. Ionization was achieved using the NCI mode using methane as the reagent gas and monitoring for ions 337 *m*/*z* for uracil and 339 *m*/*z* for [$^{15}N_2$]uracil.

Nuclear de Novo Thymidylate Synthesis—Livers from age-matched male *Shmt1*^{wt} and *Shmt1*^{tg} mice fed a standard rodent chow diet (4–6 months of age, $n = 12$ per genotype) were dissected and placed immediately in cold PBS at 5 °C. Liver extracts for each genotype group were combined for nuclei purification. The nuclei were prepared using an iodixanol gradient as previously described (8). *De novo* dTMP reactions were completed as previously described (8). In short, purified nuclei were suspended in 500 μl of nuclear assay buffer containing 5 mM NADPH (Sigma), 100 mM β-mercaptoethanol, 25 mM HEPES, pH 7.5, 50 mM sucrose, 5 mM $MgCl_2$, 25 mM KCl, and 1 mM dUMP (Sigma) and quantified using a hemocytometer. 125 μl of assay buffer containing equal numbers of suspended nuclei were aliquoted into four 1.5-ml plastic tubes, and 8 μCi of [2,3-^{3}H]-L-serine (Moravek Biochemicals) was added to each sample. The assay was conducted under three different experimental conditions: lysed nuclei, nuclei were lysed with sonication (Branson Sonifier 150) at 5 °C using two 10-s pulses at 10 watts separated by a 10-s resting interval; intact nuclei; or intact nuclei with SHMT1 inhibitor, intact nuclei incubated with aminomethylphosphonate (Sigma) added to a final concentration of 100 mM. The reactions were incubated for 12 h at 37 °C with shaking at 300 rpm. The nuclei were pelleted by centrifugation at 2000 rpm for 5 min, and the supernatant was collected and analyzed for radiolabeled thymidylate by HPLC. Sample preparation and HPLC was performed as previously described (23, 24). Fractions were collected, and tritium was quantified with a scintillation counter. The retention times of [2,3-^{3}H]-L-serine (9 min) and [^{3}H]thymidine (17 min) (Moravek Biochemicals) were verified prior to separation of the reaction mixtures. The data were normalized to the number of nuclei. All of the experiments were performed in duplicate.

Metabolite Profile from Plasma—Total homocysteine, cystathionine, total cysteine, methionine, glycine, serine, α-aminobutyric acid, *N,N*-dimethylglycine, and *N*-methylglycine were assayed in mouse plasma by stable isotope dilution capillary gas chromatography-mass spectrometry as described previously (25, 26).

Statistical Analyses—Differences in genotype distribution were analyzed by the χ^2 test. Differences between two groups were determined by Student's *t* test analysis. Differences among more than two genotypes were analyzed by two-way ANOVA and Dunnett's post hoc test using the wild type genotype as the control group. Diet × genotype effects were analyzed by two-way ANOVA and Tukey's Honestly Significant Difference post hoc test. The groups were considered significantly different when the p value ≤ 0.05. The data are presented as the mean ± S.E. All of the statistics were performed using JMP IN software, release 5.1.2.

RESULTS

Shmt1^{tg+} *Mice Are Viable*—*Shmt1* transgene expression was activated by crossing *Shmt1*^{tg} mice to Cre-expressing mice, which results in deletion of the *βgeo* cassette and relocation of the *Shmt1* intronless transgene 3′ to the β-actin promoter, generating *Shmt1*$^{tg+}$ mice (Fig. 2*A*; $^+$ denotes *Cre* positive). PCR-based genotyping results in the generation of a 542-bp PCR product for the wild type *Shmt1* allele and a 215-bp PCR product for the transgene (Fig. 2*B*).

To determine whether *Shmt1*^{tg} mice were viable upon activation of the transgene, the *Shmt1*$^{tg+}$ genotype distribution was determined from crosses between BALB/c CMV-*Cre* homozygous male mice and FVB/N *Shmt1*^{tg} female mice carrying one copy of the transgenic allele (Fig. 2*C*). A total of 226 F1 pups from 39 litters were examined (Table 1). The mean litter size was 5.8 pups, which approximates observed litter sizes for inbred FVB/N and BALB/c mice. The *Shmt1* transgene was distributed as expected for Mendelian inheritance with a ratio of *Shmt1*$^{wt+}$ to *Shmt1*$^{tg+}$ mice of 97:129, and both sexes were

TABLE 1

SHMT1 overexpressing mice are viable

Shmt1^{tg} mice were crossed with Cre-expressing mice to activate expression of the *Shmt1* transgene, and their progeny were genotyped. The expected genotype distribution was calculated based on a Mendelian distribution. Differences between observed and expected genotype distributions were analyzed by chi-squared analysis. p values ≤ 0.05 were considered significantly different. *Shmt1*$^{wt+}$, Cre^{+} *Shmt1* wild type mice; *Shmt1*$^{tg+}$, Cre^{+} *Shmt1*^{tg} mice. NS, not significant.

	Observed genotype distribution			Expected genotype distribution		
Genotype	Male	Female	Total	Male	Female	Total
Shmt1^{wt+}	55	42	97	56.5	56.5	113
Shmt1^{tg+}	70	59	129	56.5	56.6	113
Total	125	101	226	113	113	226
Number of litters observed				39		
Mean litter size (mean ± S.E.)				5.8 ± 0.4		
p value, observed *versus* expected genotype distribution				NS		
p value, observed *versus* expected sex distribution				NS		

found at the expected frequency. *Shmt1*$^{tg+}$ mice were not bred, so the effect of SHMT1 overexpression on fertility remains to be determined.

SHMT1 Protein Overexpression in Shmt1^{tg+} *Mice*—*Shmt1*$^{tg+}$ mice demonstrated variable tissue-dependent SHMT1 overexpression, as detected by immunoblotting (Fig. 3). The kidney, colon, and ileum of *Shmt1*$^{tg+}$ mice exhibited a 3–4-fold increase, whereas liver demonstrated a 2-fold increase in SHMT1 protein levels in comparison with *Shmt1*^{wt}, *Shmt*$^{wt+}$, and *Shmt1*^{tg} (not Cre activated) mice. Endogenous SHMT1 is undetectable in the brain of wild type mice by immunoblotting, but a significant amount of SHMT1 can be detected in the brain of *Shmt*$^{tg+}$ mice. Note that the lower band on the brain immunoblot is nonspecific, as is also observed in *Shmt1* null mice.

SHMT1 and Folate Status—SHMT1 overexpression did not impact plasma or liver folate status in mice fed the control or folate/choline-deficient diet (Table 2). As expected, the folate/choline-deficient diet resulted in a significant decrease in plasma and liver folate after 32 weeks on the diet (Table 2).

SHMT1, de Novo Thymidylate Synthesis and Uracil Misincorporation in Nuclear DNA—SHMT1 preferentially partitions one-carbon units to thymidylate synthesis through the SUMO-mediated localization of the thymidylate synthesis pathway to the nucleus during S phase (5, 6). Furthermore, TYMS protein levels respond to changes in SHMT1 expression; *Shmt1*$^{+/-}$ mice exhibit decreased SHMT1 and TYMS protein, decreased capacity for *de novo* dTMP synthesis, and elevated uracil in nuclear DNA (9). Therefore, we hypothesized that overexpression of SHMT1 would be associated with increased TYMS expression and increased nuclear *de novo* thymidylate synthesis capacity with a consequent decrease in uracil incorporation in nuclear DNA. Unexpectedly, *Shmt1*$^{tg+}$ mice fed the control diet demonstrated a significant 2-fold increase in uracil content in hepatic nuclear DNA (Table 2) despite an almost 4-fold increase in total liver SHMT1 (3.9 ± 0.3) and TYMS (3.7 ± 0.4) protein content in comparison with *Shmt1*$^{wt+}$ mice (1.0 ± 0.3 and 1.0 ± 0.3, respectively) (Fig. 4*A*). When placed on a folate- and choline-deficient diet, *Shmt1*$^{tg+}$ mice exhibited a 10-fold increase in nuclear uracil content compared with a 2-fold increase observed in wild type mice on the same deficient diet (Table 2). These data indicate that elevated SHMT1 and TYMS expression is not sufficient to increase capacity for *de novo* thymidylate synthesis.

To explore this unexpected finding, we sought to clarify the specific effect of SHMT1 overexpression on nuclear *de novo*

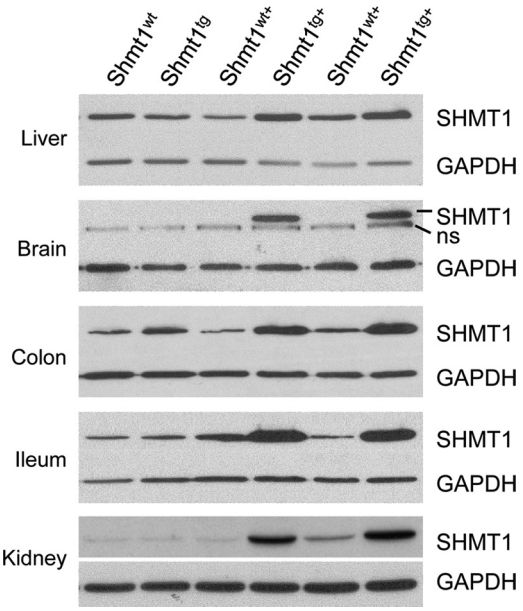

FIGURE 3. **SHMT1 protein expression in liver, brain, colon, ileum, and kidney of non-Cre-activated *Shmt1* wild type (*wt*) and transgenic (*tg*) mice (*lanes 1* and *2*, respectively), and Cre-activated *Shmt1* wild type (*wt*+, *lanes 3* and *5*) and transgenic (*tg*+, *lanes 4* and *6*) mice.** Immunoblots of tissue lysates were probed with polyclonal anti-SHMT1 and polyclonal anti-GAPDH antibodies. GAPDH served as a loading control.

thymidylate synthesis. Isolated hepatic nuclei from *Shmt1*$^{tg+}$ mice fed the folate-replete diet contained 75% less SHMT1 and TYMS protein compared with their wild type counterparts (Fig. 4, *C* and *D*), whereas SHMT1 overexpression had no effect on DHFR localization to the nucleus (Fig. 4*D*). The decrease in nuclear SHMT1 and TYMS observed in *Shmt1*$^{tg+}$ mice was associated with an approximate 50% decrease in nuclear *de novo* thymidylate biosynthesis capacity in purified hepatic nuclei (Fig. 4*B*). The decrease in *de novo* thymidylate synthesis was not due to decreased hepatic nuclear folate content because we did not observe significant differences in nuclear folate concentrations between *Shmt1*$^{wt+}$ and *Shmt1*$^{tg+}$ mice fed a standard rodent chow (9.5 ± 0.4 *versus* 10.7 ± 2.5, respectively).

Impact of SHMT1 Overexpression on Homocysteine Remethylation—SHMT1 binds 5-methylTHF in the cytoplasm, making it unavailable for the remethylation of homocysteine in cultured MCF-7 cells (14). Therefore increased SHMT1 expression is expected to result in decreased AdoMet levels and elevated homocysteine. Consistent with this expectation,

TABLE 2

Plasma and liver folate, liver *S*-adenosyl-methionine, *S*-adenosyl-homocysteine, *S*-adenosyl-methionine:*S*-adenosyl-homocysteine ratio, and uracil content in SHMT1-overexpressing mice at 32 weeks post-weaning

Differences between genotypes and diets were analyzed by Student's *t* test. nuclear DNA genotype × diet effects were analyzed by two-way ANOVA using Tukey's Honestly Significant Difference post-hoc analysis. The data represent the means ± S.E. values. *p* values ≤ 0.05 were considered significantly different. $n = 4–7$/group. Folate/choline-deficient $Shmt1^{tg+}$ mice are significantly different than control and folate/choline-deficient $Shmt1^{wt+}$ and control $Shmt1^{tg+}$ mice, $p < 0.05$, as analyzed by two-way ANOVA and Tukey's Honestly Significant Difference post-hoc test $Shmt1^{wt+}$, Cre^{+} *Shmt1* wild type mice; $Shmt1^{tg+}$, Cre^{+} $Shmt1^{tg}$ mice. NS, not significant.

Diet	*Shmt1* genotype	Plasma folate	Liver folate	AdoMet	AdoHcy	AdoMet:AdoHcy	Liver uracil
		ng/ml	*fmol/μg of protein*	*pmol/μg of protein*	*pmol/μg of protein*		*pg of uracil/μg of DNA*
AIN-93G	$Shmt1^{wt+}$	36.3 ± 7.7	43.1 ± 2.3	0.7 ± 0.2	0.4 ± 0.1	2.1 ± 0.4	0.1 ± 0.0
	$Shmt1^{tg+}$	46.8 ± 5.8	51.3 ± 3.4	0.3 ± 0.2	0.2 ± 0.2	1.2 ± 0.0	0.2 ± 0.0
AIN-93G minus folate & choline	$Shmt1^{wt+}$	7.4 ± 0.2	36.1 ± 2.6	0.7 ± 0.1	0.6 ± 0.1	1.2 ± 0.2	0.3 ± 0.0
	$Shmt1^{tg+}$	5.5 ± 1.5	34.0 ± 5.8	0.4 ± 0.0	0.6 ± 0.1	0.9 ± 0.3	2.3 ± 0.7
p value, diet effect		<0.0001	<0.0001	NS	0.006	0.04	0.01
p value, genotype effect		NS	NS	0.02	NS	0.04	0.02
p value, Diet × genotype effect		NS	NS	NS	NS	NS	0.03[1]

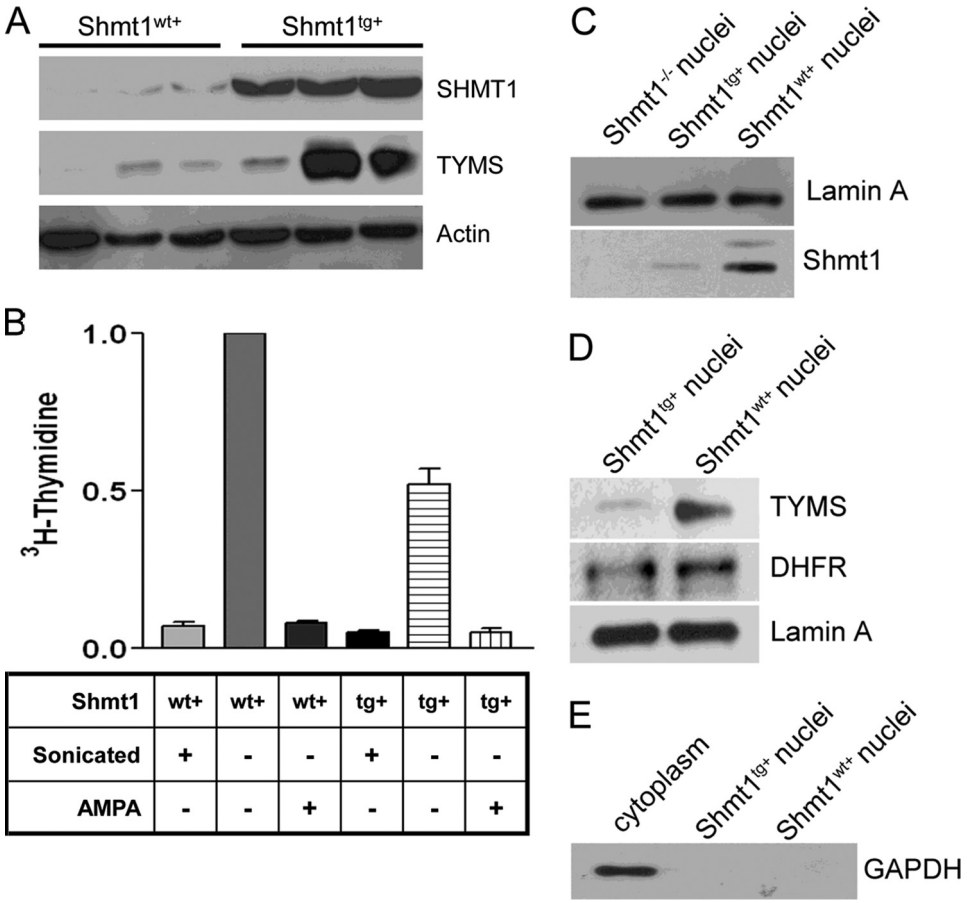

FIGURE 4. **Hepatic nuclear SHMT1, TYMS, and DHFR protein content and *de novo* dTMP biosynthesis in SHMT1 overexpressing mice.** *A*, immunoblotting for SHMT1, TYMS, and actin (loading control) from whole liver extracts from Cre-activated *Shmt1* wild type ($Shmt1^{wt+}$) and $Shmt1^{tg+}$ mice. *B*, nuclei were isolated from $Shmt1^{wt+}$ and $Shmt1^{tg+}$ mouse liver, and the capacity to convert dUMP and [2,3-^{3}H]-L-serine to [^{3}H]dTMP was determined in reactions that contained sonicated nuclei, intact nuclei, or intact nuclei incubated with 100 mM aminomethyl phosphonate, an SHMT1 inhibitor (8). *De novo* thymidylate biosynthesis activity was normalized to that of $Shmt1^{wt+}$ intact nuclei, which was assigned an arbitrary value of 1.0. The reactions were performed in duplicate, and the experiment was repeated twice. We did not observe a run-dependent difference; therefore data from the two replicate experiments were combined. The data are presented as the means ± S.E. *C* and *D*, immunoblotting for SHMT1, TYMS, and DHFR was performed on hepatic nuclei isolated from *Shmt1* null (*C* only) (3) and $Shmt1^{wt+}$ and $Shmt1^{tg+}$ mice. Lamin A was used as a nucleus-specific loading control. *E*, immunoblotting of cytoplasm-restricted GAPDH confirmed the purity of hepatic nuclei.

hepatic AdoMet and AdoMet:AdoHcy ratio, which is indicative of the cellular methylation capacity, were significantly lower in $Shmt1^{tg+}$ mice at 32 weeks post-weaning (Table 2). AdoHcy was unaffected by SHMT1 overexpression. We did not observe any genotype × diet effects on AdoMet, AdoHcy, or the AdoMet:AdoHcy ratio.

The impact of SHMT1 overexpression on homocysteine- and folate-related metabolites in the plasma of male and female mice was determined at 5 weeks post-weaning. We did not observe a significant effect of SHMT1 overexpression on any of the metabolites queried because of insufficient power to detect significant differences. A significant sex effect on plasma homocysteine, methionine, cysteine, and cystathionine was observed. Female mice exhibited increased plasma homocysteine and cysteine and decreased cystathionine and methionine relative to male mice. Plasma serine tended to be decreased in

TABLE 3

Plasma metabolic profile of SHMT1 overexpressing mice at 5 weeks post-weaning

Differences between sexes, diets, and genotypes were analyzed by Student's *t* test. Genotype × diet effects were analyzed by two-way ANOVA using Tukey's Honestly Significant Difference post-hoc analysis. The data are presented as the means ± S.E. values. *p* values ≤ 0.05 were considered significantly different. $n = 3$ males and $n = 3$ females/diet/genotype group. *Shmt1*$^{wt+}$, Cre^{+} *Shmt1* wild type mice; *Shmt1*$^{tg+}$, Cre^{+} *Shmt1*^{tg} mice. NS, not significant.

Genotype		*Shmt1*$^{wt+}$		*Shmt1*$^{tg+}$		*p* value of model effect			
Metabolite	Sex	C	FCD	C	FCD	Sex	Diet	Genotype	Diet × genotype
Homocysteine (μM)	Both	5.6 ± 0.7	7.0 ± 0.7	7.8 ± 1.3	9.9 ± 1.0	0.009	0.007	0.06	NS
	Male	4.8 ± 0.7	5.5 ± 0.2	6.6 ± 2.3	8.4 ± 0.6		0.10	NS	NS
	Female	6.4 ± 1.0	8.4 ± 0.3	9.0 ± 1.1	11.4 ± 1.6		0.03	0.08	NS
Cystathionine (nM)	Both	1697 ± 237	1687 ± 334	1552 ± 189	1555 ± 70	0.002	NS	NS	NS
	Male	1979 ± 399	2235 ± 483	1931 ± 181	1655 ± 83		NS	NS	NS
	Female	1414 ± 202	1140 ± 159	1173 ± 54	1455 ± 89		NS	NS	0.08
Cysteine (μM)	Both	171 ± 29	200 ± 20	214 ± 19	219 ± 15	<0.0001	0.006	0.10	NS
	Male	109 ± 21	158 ± 8	178 ± 15	192 ± 14		0.01	0.07	NS
	Female	232 ± 4	242 ± 12	251 ± 18	246 ± 12		NS	NS	NS
Methionine (μM)	Both	39.6 ± 5.0	29.3 ± 3.9	40.9 ± 8.8	31.4 ± 1.3	0.03	NS	0.07	NS
	Male	49.9 ± 3.7	34.6 ± 5.8	48.1 ± 18.2	32.4 ± 1.6		NS	NS	NS
	Female	29.3 ± 2.2	24.1 ± 3.7	33.7 ± 1.1	30.4 ± 2.2		0.07	NS	NS
α-Aminobutyric Acid (μM)	Both	6.8 ± 1.7	5.0 ± 0.5	4.5 ± 0.6	4.2 ± 0.3	NS	NS	NS	NS
	Male	5.8 ± 1.4	4.6 ± 0.4	5.0 ± 1.2	4.4 ± 0.5		NS	NS	NS
	Female	7.8 ± 3.3	5.4 ± 1.0	4.0 ± 0.3	4.0 ± 0.3		NS	NS	NS
Glycine (μM)	Both	312 ± 42	286 ± 22	270 ± 17	289 ± 20	0.0006	NS	NS	NS
	Male	383 ± 59	322 ± 32	291 ± 23	327 ± 6		NS	NS	NS
	Female	240 ± 12	249 ± 9	249 ± 22	250 ± 20		NS	NS	NS
Serine (μM)	Both	161 ± 21	136 ± 11	146 ± 18	134 ± 9	<0.0001	NS	0.07	NS
	Male	203 ± 17	158 ± 8	174 ± 25	151 ± 6		NS	0.07	NS
	Female	119 ± 10	113 ± 8	119 ± 16	117 ± 9		NS	NS	NS
Dimethylglycine (μM)	Both	7.8 ± 1.7	7.1 ± 0.7	6.0 ± 0.7	6.2 ± 0.8	0.0004	0.10	NS	NS
	Male	5.0 ± 0.1	5.6 ± 0.4	5.0 ± 0.7	4.6 ± 0.2		NS	NS	NS
	Female	10.5 ± 2.6	8.6 ± 0.6	7.0 ± 1.1	7.8 ± 0.5		NS	NS	NS
Methylglycine (μM)	Both	2.8 ± 0.5	2.1 ± 0.2	1.4 ± 0.1	2.0 ± 0.3	NS	0.04	NS	0.06
	Male	2.3 ± 0.5	2.3 ± 0.3	1.4 ± 0.1	1.6 ± 0.1		0.02	NS	NS
	Female	3.3 ± 1.0	1.8 ± 0.2	1.3 ± 0.1	2.4 ± 0.7		NS	NS	0.07

Shmt1^{tg+} mice, an effect driven by samples from male mice (Table 3). The folate/choline-deficient diet was associated with increased plasma homocysteine and cysteine and decreased methylglycine (Table 3). We did not observe any significant genotype × diet effects on any of the queried metabolites.

DISCUSSION

Our study demonstrates that nuclear localization of the *de novo* dTMP synthesis pathway is essential to prevent uracil accumulation in nuclear DNA and thereby maintain genome stability and confirms previous studies demonstrating that SHMT1 expression is an important determinant of uracil accumulation in DNA. The results demonstrate unequivocally that restricting the *de novo* dTMP synthesis pathway to the cytoplasm results in elevated uracil accumulation into nuclear DNA.

Shmt1^{tg+} mice demonstrated a 2–4-fold increase in SHMT1 and TYMS protein in tissues that normally express SHMT1, namely the liver, kidney, and gastrointestinal tract (Fig. 3). No significant differences in genotype distribution among Cre-activated F1 wild type or transgenic pups were observed (Table 1), indicating that the achieved level of SHMT1 overexpression had no impact on embryo survival in dams fed a standard rodent chow diet. It will be of interest to determine the effect of a folate deficient diet on *Shmt1*$^{tg+}$ embryo development, because we have demonstrated folate-responsive neural tube defects in *Shmt1* heterozygous null mice, which was attributed to reduced *de novo* thymidylate synthesis (10).

Shmt1$^{+/-}$ mice have been reported to exhibit increased uracil content in hepatic nuclear DNA, reduced levels of nuclear SHMT1 and TYMS, and consequent decreased capacity for *de novo* thymidylate synthesis (3, 9). In this study, contrary to expectations, uracil content in hepatic nuclear DNA was increased in *Shmt1*$^{tg+}$ mice compared with wild type mice, which was exacerbated markedly by a folate- and choline-deficient diet. Indeed, hepatic nuclear DNA uracil content in *Shmt1*$^{tg+}$ mice fed the control diet was comparable with that observed in *Shmt1*$^{+/-}$ mice (3, 9). Compared with wild type mice, *Shmt1*$^{tg+}$ mice exhibited a 4-fold increase in total hepatic SHMT1 and TYMS protein expression, whereas nuclear localization of SHMT1 and TYMS was reduced by ~75%, resulting in a 50% reduction in dTMP synthesis in isolated nuclei from folate-replete mice (Fig. 4). Although *Shmt1*$^{tg+}$ have severalfold increased expression of SHMT1 and TYMS compared with *Shmt*$^{+/-}$ mice, they both exhibit decreased levels of nuclear SHMT1 and TYMS protein, reduced nuclear thymidylate synthesis, and elevated uracil in DNA compared with wild type mice. Collectively, these results indicate that nuclear localization of the *de novo* thymidylate biosynthesis pathway is essential for maintaining sufficient thymidine nucleotide pools for DNA replication.

The mechanism by which SHMT1 and TYMS accumulation in the nucleus is inhibited in *Shmt1*$^{tg+}$ mice is not known. Elevated expression of SHMT1 in the cytoplasm may impair sumoylation of SHMT1 and/or TYMS or prevent their translocation into the nucleus. Interestingly, the accumulation of SHMT1 and TYMS, but not DHFR, in the nucleus is coordinated and dependent on SHMT1 expression.

Similar to our previous studies, in which SHMT1-dependent expression of TYMS was observed in colon and embryonic tissue (9, 10), the present study provides additional evidence for the coregulation of these two proteins. *Shmt1*$^{-/+}$ mice were shown to have ~50% SHMT1 protein content, which was con-

comitant with a reduction in TYMS (9). Interestingly, SHMT1, TYMS, and thymidine kinase 1 protein expression were also responsive to folate deficiency as demonstrated by their increased expression in mice fed the folate/choline-deficient diet (9). Microarray analysis did not indicate significant transcriptional changes to TYMS expression in *Shmt1*$^{-/+}$, suggesting that their coregulation occurs post-transcriptionally (9). We also have not queried the effect of SHMT1 expression on sumoylation of itself or TYMS, a mode by which SHMT1 could influence nuclear translocation. The mechanism by which SHMT1 expression influences TYMS levels is actively being investigated.

This study also confirms that increased SHMT1 expression plays a modest role in the regulation of homocysteine methylation in the cytoplasm. SHMT1 is a 5-methylTHF binding protein (27), and therefore overexpression of SHMT1 was anticipated to reduce hepatic methionine and AdoMet synthesis by sequestering cytoplasmic 5-methylTHF. Consistent with this expectation, SHMT1 overexpression decreased hepatic AdoMet, which resulted in a reduced AdoMet:AdoHcy ratio (Table 2). SHMT1 overexpression did not have a major impact on serum one-carbon metabolites, because our study was underpowered to detect significant differences.

We previously demonstrated that the common human L474F variant impairs the UBC9-SHMT1 interaction and consequently SHMT1 sumoylation and translocation to the nucleus (5). The impact of this SHMT1 variant on TYMS nuclear localization and nuclear *de novo* thymidylate biosynthesis capacity is unknown. The reduction of nuclear *de novo* dTMP synthesis capacity in the *Shmt1*$^{tg+}$ mouse provides a unique experimental model of the human L474F SHMT1 variant and permits mechanistic studies that investigate and validate reported epidemiological associations of this variant with lung cancer and cardiovascular risk (11–13).

Acknowledgments—We acknowledge Martha Field, Anna Beaudin, Sylvia Allen, and Rachel Slater for technical assistance.

REFERENCES

1. Goulian, M., Bleile, B., and Tseng, B. Y. (1980) *Proc. Natl. Acad. Sci. U.S.A.* **77,** 1956–1960
2. Blount, B. C., Mack, M. M., Wehr, C. M., MacGregor, J. T., Hiatt, R. A., Wang, G., Wickramasinghe, S. N., Everson, R. B., and Ames, B. N. (1997) *Proc. Natl. Acad. Sci. U.S.A.* **94,** 3290–3295
3. MacFarlane, A. J., Liu, X., Perry, C. A., Flodby, P., Allen, R. H., Stabler, S. P., and Stover, P. J. (2008) *J. Biol. Chem.* **283,** 25846–25853
4. Anderson, D. D., Quintero, C. M., and Stover, P. J. (2011) *Proc. Natl. Acad. Sci. U.S.A.* **108,** 15163–15168
5. Woeller, C. F., Anderson, D. D., Szebenyi, D. M., and Stover, P. J. (2007) *J. Biol. Chem.* **282,** 17623–17631
6. Anderson, D. D., Woeller, C. F., and Stover, P. J. (2007) *Clin. Chem. Lab. Med.* **45,** 1760–1763
7. Ching, Y. H., Munroe, R. J., Moran, J. L., Barker, A. K., Mauceli, E., Fennell, T., Dipalma, F., Lindblad-Toh, K., Abcunas, L. M., Gilmour, J. F., Harris, T. P., Kloet, S. L., Luo, Y., McElwee, J. L., Mu, W., Park, H. K., Rogal, D. L., Schimenti, K. J., Shen, L., Shindo, M., Shou, J. Y., Stenson, E. K., Stover, P. J., and Schimenti, J. C. (2010) *BMC Genet.* **11,** 106–116
8. Anderson, D. D., and Stover, P. J. (2009) *PLoS One* **4,** e5839
9. MacFarlane, A. J., Perry, C. A., McEntee, M. F., Lin, D. M., and Stover, P. J. (2011) *Cancer Res.* **71,** 2098–2107
10. Beaudin, A. E., Abarinov, E. V., Noden, D. M., Perry, C. A., Chu, S., Stabler, S. P., Allen, R. H., and Stover, P. J. (2011) *Am. J. Clin. Nutr* **93,** 789–798
11. Lim, U., Peng, K., Shane, B., Stover, P. J., Litonjua, A. A., Weiss, S. T., Gaziano, J. M., Strawderman, R. L., Raiszadeh, F., Selhub, J., Tucker, K. L., and Cassano, P. A. (2005) *J. Nutr.* **135,** 1989–1994
12. Wernimont, S. M., Raiszadeh, F., Stover, P. J., Rimm, E. B., Hunter, D. J., Tang, W., and Cassano, P. A. (2011) *J. Nutr.* **141,** 255–260
13. Piskac-Collier, A. L., Monroy, C., Lopez, M. S., Cortes, A., Etzel, C. J., Greisinger, A. J., Spitz, M. R., and El-Zein, R. A. (2011) *Genes Chromosomes Cancer* **50,** 1–12
14. Herbig, K., Chiang, E. P., Lee, L. R., Hills, J., Shane, B., and Stover, P. J. (2002) *J. Biol. Chem.* **277,** 38381–38389
15. Perry, C., Sastry, R., Nasrallah, I. M., and Stover, P. J. (2005) *J. Biol. Chem.* **280,** 396–400
16. Woeller, C. F., Fox, J. T., Perry, C., and Stover, P. J. (2007) *J. Biol. Chem.* **282,** 29927–29935
17. Fox, J. T., Shin, W. K., Caudill, M. A., and Stover, P. J. (2009) *J. Biol. Chem.* **284,** 31097–31108
18. Nakshatri, H., Bouillet, P., Bhat-Nakshatri, P., and Chambon, P. (1996) *Gene* **174,** 79–84
19. Novak, A., Guo, C., Yang, W., Nagy, A., and Lobe, C. G. (2000) *Genesis* **28,** 147–155
20. Liu, X., Szebenyi, D. M., Anguera, M. C., Thiel, D. J., and Stover, P. J. (2001) *Biochemistry* **40,** 4932–4939
21. Stover, P. J., Chen, L. H., Suh, J. R., Stover, D. M., Keyomarsi, K., and Shane, B. (1997) *J. Biol. Chem.* **272,** 1842–1848
22. Bensadoun, A., and Weinstein, D. (1976) *Anal. Biochem.* **70,** 241–250
23. Field, M. S., Szebenyi, D. M., and Stover, P. J. (2006) *J. Biol. Chem.* **281,** 4215–4221
24. Friso, S., Choi, S. W., Dolnikowski, G. G., and Selhub, J. (2002) *Anal Chem.* **74,** 4526–4531
25. Stabler, S. P., Lindenbaum, J., Savage, D. G., and Allen, R. H. (1993) *Blood* **81,** 3404–3413
26. Allen, R. H., Stabler, S. P., and Lindenbaum, J. (1993) *Metabolism* **42,** 1448–1460
27. Stover, P., and Schirch, V. (1991) *J. Biol. Chem.* **266,** 1543–1550